Ultra-sensitive chemical and biological analysis via specialty fibers with built-in microstructured optofluidic channels

Zhang, Nan; Li, Kaiwei; Cui, Ying; Wu, Zhifang; Shum, Perry Ping; Auguste, Jean-Louis; Dinh, Xuan Quyen; Humbert, Georges; Wei, Lei

2018

https://hdl.handle.net/10356/90136

https://doi.org/10.1039/C7LC01247K

Ultra-sensitive chemical and biological analysis via specialty fibers with built-in microstructured optofluidic channels

Nan Zhang,[†ab] Kaiwei Li,[†a] Ying Cui,[ab] Zhifang Wu,[ab] Perry Ping Shum,[ab] Jean-Louis Auguste,[c] Xuan Quyen Dinh,[bd] Georges Humbert[*c] and Lei Wei[*ab]

All-in-fiber optofluidics is an analytical tool that provides enhanced sensing performance with simplified analyzing system design. Currently, its advance is limited either by complicated liquid manipulation and light injection configuration, or by low sensitivity resulted from inadequate light-matter interaction. In this work, we design and fabricate a side-channel photonic crystal fiber (SC-PCF) and exploit its versatile sensing capabilities in in-line optofluidic configurations. The built-in microfluidic channel of SC-PCF enables strong light-matter interaction and easy lateral access of liquid samples in these analytical systems. In addition, the sensing performance of SC-PCF is demonstrated with methylene blue for absorptive molecular detection, and with human cardiac troponin T protein utilizing a Sagnac interferometry configuration for ultra-sensitive and specific biomolecular specimen detection. Owing to the features of great flexibility and compactness, highly-sensitive to the analyte variation, and efficient liquid manipulation/replacement, the demonstrated SC-PCF offers a generic solution to be adapted to various fiber-waveguide sensors to detect a wide range of analyte in real time, especially for the applications from environment monitoring to biological diagnosis.

Introduction

Optofluidics, as the integration of photonics and microfluidics, combines the optical analytic methods and sample delivery into one system.[1–4] Especially, with the advance of micro/nano fabrication technology, it has been widely applied in the chemical and biological sensing fields to provide enhanced sensing capabilities with ultra-small sample consumption volume.[5–7] Compared with on-chip waveguides, all-in-fiber optofluidic sensing systems offer the following distinctive features: immunity to electromagnetic interference, being free standing, miniature and light weight, easy light coupling, low waveguide losses, and low cost for mass production.[8–10] In particular, photonic crystal fibers (PCFs), which serve as both low-loss waveguide and microfluidic channel, show their instinctive advantages in constructing all-in-fiber optofluidic sensors.[11–13] The tiny voids running along the entire length of fiber are the natural chambers for hosting the liquid fluid with extremely low volume for microanalysis, while avoiding contamination. The advanced fabrication technique enables large freedom in tuning its wave-guidance properties and great consistency in the fiber geometry over long length. Therefore, the use of PCF facilitates more compact sensing configurations, and unprecedented long light-analyte interaction compared with other fiber sensors, for example, microfibers.[14]

Facing the increasing demand of ultra-sensitive molecular analysis with the applications from environmental monitoring to biological diagnosis, a few PCF geometries have been adopted for in-line biochemical sensing. However, most of these fibers are not specially designed for in-line liquid sensing and the performance is still limited by a few factors. 1) Low sensitivity due to weak light-matter interaction and low coupling efficiency. Though, a few fiber geometries, including hollow-core PCFs[15] and suspended-core PCFs,[16] are able to provide large overlap between light and matter in the large core area, difficulties in light coupling due to mismatch of modal profile and large core-size contrast with single mode fibers (SMFs) compromises its sensing performance when integrated into all-in-fiber systems. 2) Complex techniques in creating in-line liquid access. Currently, making liquid side-access requires the assistance of either a precisely fabricated connecter placed in-between the PCF and SMFs[12] or using complicated micro-machining techniques, such as femtosecond/CO_2 laser with high-accuracy positioning stages,[17,18] to form holes on the fiber surface.

To address the aforementioned challenges and difficulties, we design and fabricate a side-channel photonic crystal fiber (SC-PCF) which composes of a large yet well-defined side-channel in the fiber lattice cladding and a fiber core directly exposed to the side-channel, which allows easy infiltration of liquid samples, convenient light coupling and strong light-analyte interaction when splicing the SC-PCF to side-polished

a. School of Electrical and Electronic Engineering, Nanyang Technological University, Singapore. E-mail: WEI.LEI@ntu.edu.sg
b. CINTRA CNRS/NTU/THALES, UMI 3288, 50 Nanyang Drive, Singapore.
c. XLIM Research Institute - UMR 7252 CNRS/University of Limoges/CNRS, 123 Avenue Albert Thomas, Li¬moges Cedex, France. E-mail: georges.humbert@xlim.fr
d. Thales Solutions Asia Pte Ltd, R&T Centre, 28 Changi North Rise, Singapore
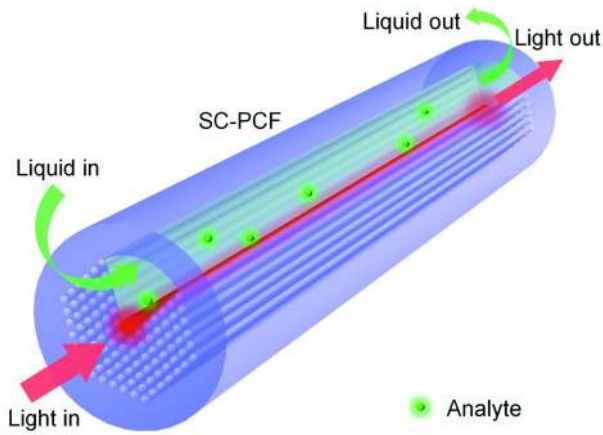† These authors contribute equally to this paper.

Figure 1. Schematic diagram of liquid sensing with SC-PCF (Dimensions not to scale).
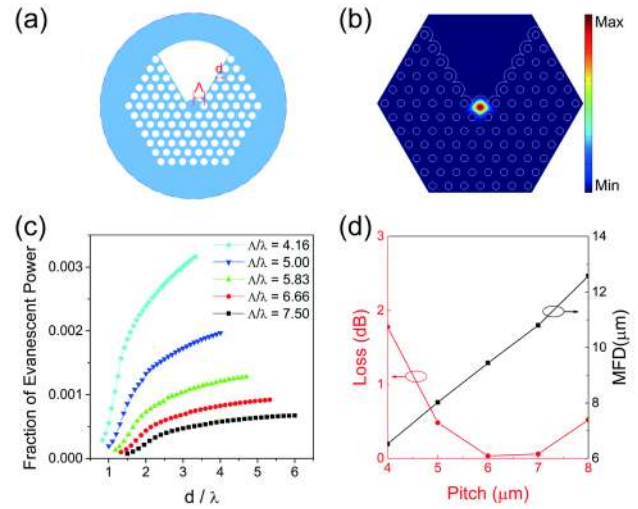

Figure 2. (a) Geometry of SC-PCF. Blue color indicates silica material, and white regions represent air channels. (b) Simulated mode energy distribution of HE_{11} core mode. (c) FP_{ch} in the side-channel against d normalized to wavelength for different Λ. (d) Calculated butt-coupling loss and MFD variations of SC-PCF against Λ (for a wavelength of 1550 nm).

SMFs. The schematic diagram of the SC-PCF for liquid sensing is depicted in Fig. 1. By characterization, a fast in-line liquid flow circulation rate of 0.4 μL/min in the fiber side-channel can be easily achieved with the fabricated SC-PCF fiber sample. Moreover, the flexible SC-PCF exhibits very low bending loss, and it can be adapted to various in-line fiber-waveguide sensing schemes to detect a wide range of analytes. For demonstration, we integrate the SC-PCF into an all-in-fiber in-line optofluidic absorption sensing configuration and a Sagnac interferometer sensing scheme and they show high performance for optical absorption spectroscopy, liquid refractive index (RI) measurement and human cardiac troponin T (cTnT) protein detection, respectively.

Methods

Fiber design and simulation

The SC-PCF is designed as shown in Fig. 2(a). It has a solid core with 6 rings of air holes arranged in triangular lattice. One-sixth of the cladding air-hole is left empty and forms a relatively large air channel at the side of the fiber core. An outside thick layer of silica wall protects the fiber core from contamination and maintains sufficient mechanical strength. To control the evanescent power in the fiber side-channel, we theoretically investigate the dependency of the fraction of power in the side-channel FP_{ch} (ratio of light power in the side-channel P_{ch} over the total power P_{all} of the core mode) on fiber geometric parameters, including hole-diameter d and pitch Λ (hole to hole distance). Simulations are carried out with finite element method (COMSOL 3.5). The RI of fiber material (silica) is calculated from its Sellmier equation.[19] Since we aim for liquid-based sensing, the indices of air holes and the side-channel are 1 (air) and 1.33 (water), respectively.

The simulated mode energy distribution of fundamental core mode (HE_{11}) is shown in Fig. 2(b). The variation trends of FP_{ch} against hole-diameter d under different Λ (both are normalized to wavelength λ), plotted in Fig. 2(c), indicate that FP_{ch} can be enlarged by decreasing Λ and increasing d.

Because smaller Λ and larger d correspond to smaller fiber core size, which allows a higher ratio of evanescent-field power to penetrate into the side-channel. Another factor that needs to be considered in the fiber geometry design is the connection loss to SMF since we aim to integrate the SC-PCF in an all-in-fiber system. The butt-coupling loss (α) of the SC-PCF with standard SMF can be approximately calculated by the following equation:[20]

$$\alpha = -20 log \left((2d_{SMF}d_{SC-PCF})/(d_{SMF}^2 + d_{SC-PCF}^2) \right) \quad (1)$$

where d_{SMF} and d_{SC-PCF} are the mode field diameters (MFDs) of the SMF and SC-PCF, respectively. MFD corresponds to the region diameter where the light power drops to $1/e^2$ of the maximum value. Simulation results show that MFD of SC-PCF is proportional to the fiber pitch Λ as indicated by the black square attached to the right Y-axis in Fig. 2(d). For a given wavelength, the MFD of SC-PCF relies on the fiber pitch and the MFD of SMFs is constant, thus the butt-coupling loss of the SC-PCF and standard SMF is affected by the pitch of SC-PCF. The butt-coupling loss against Λ estimated by Eq. (1) is plotted as red solid circle in Fig. 2(d), indicating a minimum loss can be achieved at the pitch of ~6 μm.

Therefore, to balance the fraction of evanescent power in the side-channel and the coupling loss to SMF, and get single mode propagation in the fiber core,[21] the value of Λ and d/Λ are selected to be 6 μm and 0.43, respectively. The response of effective refractive indices (n_{eff}) of the HE_{11} mode to RI variation in the fiber side-channel plotted in Fig. S1 suggests that with the increasing of liquid RI, both n_{eff} of the HE_{11} mode and FP_{ch} value increase.

Fiber fabrication

SC-PCF is fabricated using a 2-steps stack-and-draw process.[22] The preform of SC-PCF is first drawn into intermediate canes. Then the cane is inserted into a glass tube and drawn into fibers. To prepare the large fiber preform, small capillaries are

first fabricated by drawing large tubes. The ratio of inner diameter to outer diameter of the tube should be the same as the value of d/Λ of the fiber. Then, the fabricated capillaries and the fiber core rod are stacked together to form the preform of SC-PCF. The fiber map design is shown in Fig. S2. To stabilize the preform and the structure of SC-PCF during the drawing process, both ends of the preform are fully filled, leaving a segment of 40 cm long SC-PCF structure in the middle of the preform, as shown in Figure S3 and S4. During the drawing process, both drawing speed and furnace temperature need to be controlled precisely to maintain the geometry of SC-PCF.

Preparation of in-line inlet/outlet with SC-PCF

The fabricated SC-PCF is spliced with side-polished SMFs to enable simultaneous lateral liquid access to the side-channel and light injection to the fiber core, as depicted in the inset of Fig. 4(a). To expose the side-channel only and seal the rest of the small air holes in SC-PCF, SMFs are deliberately polished from one side to a position that is ~ 36 μm from the center of the fiber core using a polish machine (Buehler, MetaServ 250). During splicing, the direction of the fiber side-channel needs to be aligned accurately with the polished side of the SMFs. To enable fast liquid infiltration, a polydimethylsiloxane (PDMS, Dow corning, Sylgard 184) block with a 1.4-mm-diameter circular window on the top, a glass plate, and a Teflon tube are used to provide a liquid insertion inlet/outlet with the connection to a liquid pool/syringe pump. Extra PDMS is used to seal the empty space between fiber and glass plate to avoid liquid leakage. The syringe pump (Ristron, RSP02-B) works in imbibition mode in the following experiments. With the assistance of the syringe pump, the solutions are injected from the inlet, and extracted from the outlet after flowing through the side-channel of the SC-PCF over the entire fiber length.

Antibody immobilization and cTnT protein detection

The immobilization of cTnT antibody on the fiber core surface follows a modified method that utilizes electrostatic interaction.[23,24] First, a 5 mM sodium hydroxide (NaOH, Alfa Aesar) solution is prepared and infiltrated into the side-channel for 10 mins to immobilize a layer of OH- group on the fiber inner surface, followed by a 20-mins deionized (DI) water rinse to remove redundant NaOH solutions. Second, a monolayer of poly (allylamine) (PAA, Sigma-Aldrich, Molecular weight: ~65000) is deposited on the core surface through electrostatic interaction, since PAA is positively charged. In this step, PAA (0.5 %) solution flow through the side-channel for 30 mins for thorough adsorption and then rinsed with DI water for another 20 mins. Next, the side-channel of the fiber is pumped with a phosphate buffered saline (PBS, Vivantis, pH 7.4) solution for 20 mins to get ready for the immobilization of active cTnT antibody. Third, a layer of active cTnT antibody (Abcam) is introduced to the core surface through chemical binding with PAA by infiltration of a 10 μg/mL cTnT antibody solution for 1 h and PBS rinse for 30 mins. Fourth, to prevent non-specific binding, bovine serum albumin (BSA, Aladdin) solution with a concentration of 1 mg/mL is added and

incubated for 30 mins to block un-reacted binding sites. Afterwards, PBS rinsing is carried out for 30 mins. In the final step, a group of cTnT protein (Abcam) solutions (concentration ranges from 1 pg/mL onwards) are pumped into the side-channel to characterize its sensing capability and the limit of detection (LOD). Each concentration is continuously infiltrated for 20 mins for sufficient binding. Rinsing steps are performed to remove un-adsorbed molecules.

Results and discussions

Fiber fabrication and characterization

The microscope photo of the intermediate cane and the scanning electron microscope (SEM) image of the fabricated SC-PCF cross section are shown in Fig. 3(a) and 3(b). The outer diameter, the size of the side-channel, Λ, and d/Λ of the fabricated fiber are measured to be 118 μm, 30 μm, 6.08 μm, and 0.6, respectively. Fig. 3(c) shows the energy distribution of HE_{11} mode at 1530 nm captured with a camera at the fiber output end. The mode energy obeys Gaussian distribution, and agrees with the simulated mode profile shown in Fig. 2(b).

The transmission loss of SC-PCF at 1550 nm is measured to be 0.27 dB/m by a cutting back method from a fiber length of 5 m. The total insertion loss after splicing with an SMF is measured to be less than 1 dB by using a broadband source (Infinon Research, IRBL-11111-F) and an optical spectrum analyzer (OSA, Yokogawa, AQ6370C), as presented in Fig. 3(d). The transmission spectrum of a 10 cm-long SC-PCF is plotted as the black curve in Fig. 3(d). After inserting a section of SMF by butt-coupling, the transmission power drops by about 0.22 dB as the red curve at 1550 nm. After fusion arc splicing (Sumitomo electric, TYPE-36), the transmission power drops
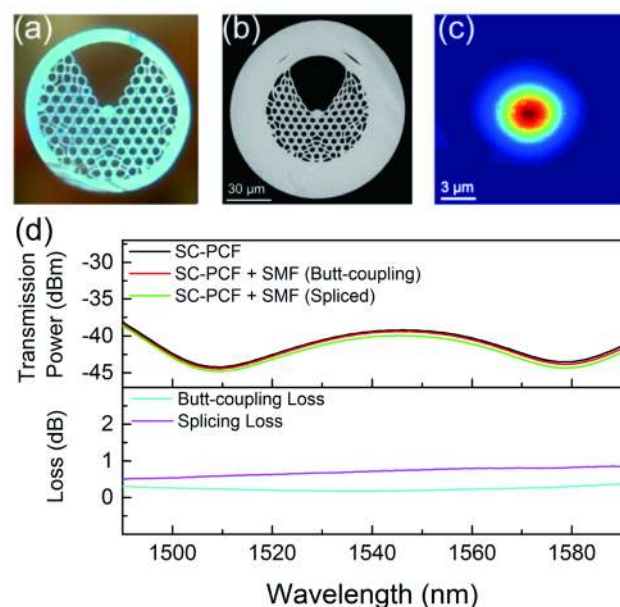

Figure 3. (a) Microscope photo of the fabricated cane. (b) SEM image of the fabricated fiber. (c) Measured energy distribution of fundamental mode at 1530 nm through butt-coupling with SMFs. (d) Transmission spectra collected for loss analysis of the splicing.

about another 0.54 dB as the green curve. The light blue and purple curves are the losses caused by the butt-coupling and splicing, respectively.

Next, the bending loss of SC-PCF is investigated as well since it is related to the flexibility and stability of the sensing system. A distributed feedback laser source at 1530 nm is launched into a 2-m-long SC-PCF through SMF splicing at one fiber end. After passing through the SC-PCF which is wrapped around a 0.5-inch-diameter rod, the near-filed transmitted mode profile is captured at the output end of SC-PCF with a 20x objective lens and an InGaAs camera, and the transmitted power is recorded for analysis as well. The transmitted mode profiles under the conditions of without wrapping, with 5-coil wrapping and 10-coil wrapping around a 0.5-inch rod show no obvious deformation (shown in Fig. S5). The transmitted laser powers are measured to be -4.11, -4.27 and -4.35 dBm, respectively. A power drop of 0.2 dB after 10-coil wrapping indicates an ultralow bending loss of the SC-PCF. The measured low transmission loss together with the ultra-low bending loss of SC-PCF are preferable features for constructing high-performance all-in-fiber sensing scheme, especially when long fiber length is necessary for enhancing sensing.

In-line flow rate characterization

We characterize the flow rate of the water flowing through the side-channel of SC-PCF after splicing with side polished SMFs, as water is a widely used solvent for chemical and biological samples. We observe that the time cost for a 40-µL water plug to flow through the side-channel is ~ 100 mins, indicating a flow rate (r) of ~0.4 µL /min.
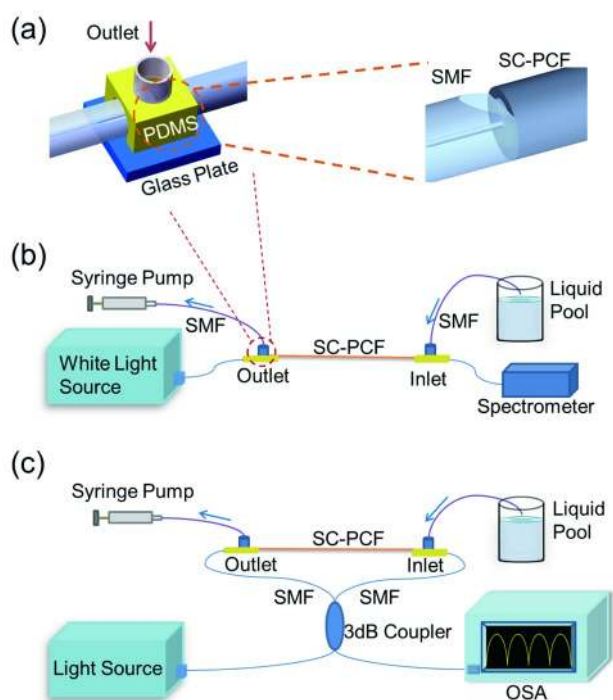
Figure 4. (a) Details of the splicing point of the SC-PCF to side-polished SMFs. (b) Scheme of the absorption experiment. (c) Scheme of the Sagnac interferometer.
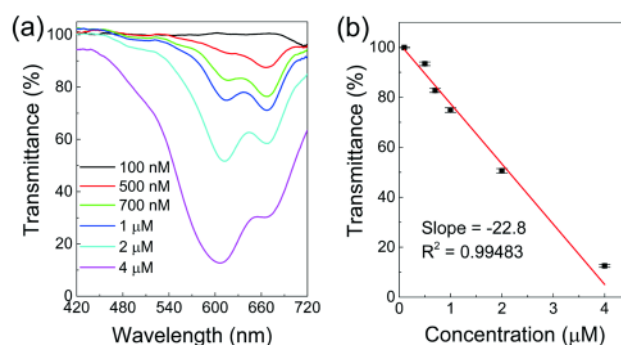
Figure 5. (a) Transmission spectra for different concentrations of MB solutions. (b) Transmittance at 605 nm for different concentrations. The error bars are the standard deviation calculated based on 5 independent measurements. The red straight line is linearly fitted to the experimental data.

In-line absorption sensing

Absorption sensing is a generic way to detect absorptive molecules, which is widely extended to realize chemical and biological molecule detections through specific chemical bindings, providing easy sensing configuration and material processing procedure.[25,26] In particular, methylene blue (MB), as active and powerful dye molecule, has shown promising applications in DNA-based diagnose,[27] pH sensing[28] and water testing[29] etc. Highly integrated absorption sensing is highly desirable owing to its advantages of short assay time and low sample consumption. However, it has been limited by difficulties in light coupling and in-line samples replacement. Our SC-PCF based all-in-fiber in-line sensing configurations can provide an easy solution for quantitative absorption sensing since fast in-line liquid circulation, and stable and high coupling efficiency can be realized through direct splicing with side-polished SMFs. To verify the absorption sensing capability of this SC-PCF, we infiltrate a group of MB (Sigma-Aldrich) aqueous solutions with concentrations ranging from 1 nM onwards into the side-channel of a 535 mm-long SC-PCF in an ascending order of concentration, and use a spectrometer (Ocean, USB 2000) to monitor the transmittance of a white light source (Ando, AQ-4303B) after passing through the SC-PCF. As the diameter of the fiber side-channel is ~ 30 µm, the volume of detection is calculated to be ~ 0.378 µL. The scheme is plotted in Fig. 4(b). We can observe from transmission spectra plotted in Fig. 5(a) that no obvious absorption peaks under extreme low MB concentrations (below 100 nM). When the concentration increases to 500 nM, distinct absorption peaks appear in the transmission spectra, which match with the MB absorption peaks.[30,31] This indicates that the LOD of the MB absorption sensing is around 500 nM. To analyze the capability of quantitative measurements, we trace the transmittance variation at 605 nm and plot in Fig. 5(b). The good linearity and repeatability of transmittance over the concentration range of 500 nM to 4 µM reveal that this SC-PCF based absorptive platform can serve as a stable, easy-handling, and quantitative absorption sensor. In addition, the sensitivity and LOD of the absorption can be enhanced through increasing fiber length. Taking advantage of various fluorescent markers and chemical binding mechanisms, this

Lab on a Chip   **Paper**

absorption sensing platform can be easily adapted to quantitative detection of specific molecules.

Sagnac RI sensing

SC-PCF supports fast liquid circulation and sensitive modal effective refractive index (ERI) response to RI variation in the fiber side-channel. Taking advantages of these features, an in-line optofluidic Sagnac interferometer using SC-PCF is proposed here to achieve versatile and ultra-sensitive sensing capabilities. The scheme is shown in Fig. 4(c). The measured transmission spectra with/without water infiltration are plotted in Fig. S6. The interference period for air infiltration and selective water infiltration in the SC-PCF side-channel are measured to be 10.75 nm and 16.36 nm near the wavelength of 1500 nm, indicating a modal birefringence coefficient of 4.17×10^{-4} and 2.77×10^{-4}, respectively (Theory in supporting information), given that fiber length is 535 mm.

First, we characterize the RI sensing capability of the Sagnac interferometer. We infiltrate different RI solutions (RI values are measured with Reichert refractometer) into the fiber side-channel and record the spectra for analysis. Selected spectra for the RI range of 1.3322-1.3371 are plotted in Fig. 6(a). The resonance wavelength reveals a red shift when the liquid RI in the side-channel increases. To analyze its RI sensitivity, we trace the resonance wavelength shift initiating from 1549.45 nm when the RI of liquid in the side-channel equals to 1.3322, and plot the averaged resonance wavelength together with standard deviations based on 5 measurements in Fig. 6(b). Over the RI range of 1.3322-1.3371, the resonance shows a linear response to the RI variation of liquid circulated in the side-channel, and a high RI sensitivity of 2849 nm/RIU. The small standard deviation indicates the high stability of the sensing system. This sensitivity is comparable to other highly-sensitive PCF based RI sensors.[11] The detection limit (DL) is calculated to be ~8×10^{-5} given that the full-width at half-max ($\Delta\lambda_{FWHM}$) value is measured to be 1.08 nm and the value of signal to noise ratio (SNR) can be estimated as 20 dB from the spectra near the resonance wavelength of 1549.45 nm (See supporting information). The unique characteristics of enabling continuous liquid circulation, sensitive spectrum response to the RI variation surrounding the fiber core and high sensing resolution make this all-in-fiber system a potential platform for bio-sensing applications.

Human cardiac troponin T sensing

Last, we demonstrate the capability of this SC-PCF based Sagnac interferometer for in-line immunoassay with human cTnT protein as a model biomarker. cTnT is a cardiac regulatory protein, and raised cTnT concentration in serum is regarded as a standard biomarker for accurate, sensitive and specific diagnosis of acute myocardial infarction (AMI).[32] Therefore, the concentration measurement of cTnT protein is an essential method for earlier diagnosis of AMI in patients.[33] The specific detection of cTnT protein can be carried out by utilizing the biological binding of antibody and antigen. Spectra are recorded *in situ* at each step of biological binding, as plotted in Fig. S7 when signals are stable. The initial resonance
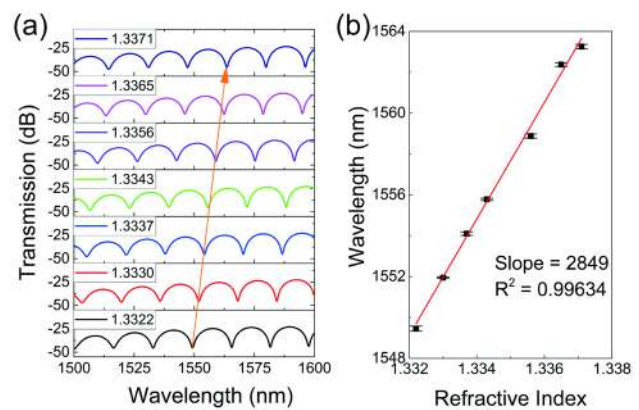

Figure 6. (a) Transmission spectra for the liquid RI range of 1.3322-1.3371. (b) Resonance wavelengths with error bars, which are traced from the RI spectra with an initial wavelength of 1549.45 nm. The error bars are the standard deviation calculated based on 5 independent measurements. The red line is linearly fitted to the experimental data.
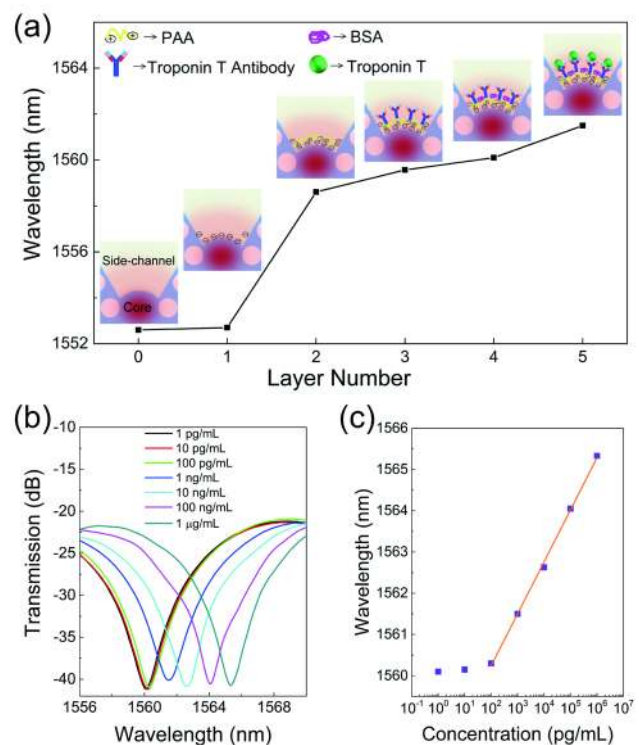

Figure 7. (a) Shift of resonance wavelength monitored at various surface treatment steps (after rinsing thoroughly). The concentration of cTnT protein is 1 ng/mL. Insets are the illustrations of the binding profiles inside the side-channel. Red color region represents the mode profile in the fiber core and evanescent wave that extended to the side-channel. (b) Shift of transmission spectra near the resonant wavelength of 1560 nm corresponding to the binding effect of different concentrations of cTnT antigen. (c) Resonant wavelengths extracted from the spectra. The purple squares indicate experimental data and the orange straight line is linearly fitted to the experimental data.

wavelength at 1552.6 nm is selected for monitoring when the side-channel is full of DI water. The resonant wavelengths after each layer deposition are summarized in Fig. 7(a) and the insets illustrate the corresponding molecule binding procedure. The resonance wavelength exhibits a red shift

along the adsorption of addition layer of molecules onto the core surface. This phenomenon agrees well with the RI sensing results, since the binding of additional layer of molecules increases the ambient RI surrounding the fiber core in the side-channel. There is a significant wavelength shift of ~1.0 nm after the binding of 10 μg/mL antibody solutions, and an extra red shift of ~0.5 nm after the BSA layer is introduced. Fig. 7(b) and 7(c) show the spectra and resonance wavelength shift under different concentrations of cTnT antigen solutions (concentration increases from 1 pg/mL) infiltrated into the fiber side-channel in the final step. For the additional layer of cTnT protein, no obvious wavelength shift is observed until the concentration of cTnT protein is increased to 1 ng/mL. Therefore, 1 ng/mL cTnT protein is the LOD of this Sagnac interferometer with a wavelength shift of ~1.4 nm. Above the concentration of 1 ng/mL, the resonance peak shifts to longer wavelength with higher antigen concentrations, reflecting the fact that more antigen molecules are adsorbed onto the core surface.

Conclusions

To address the challenges in realizing compact and ultra-sensitive all-in-fiber optofluidic sensing platforms, we design, fabricate and characterize an SC-PCF. The SC-PCF consists of a large channel at one side of the fiber core to enable fast liquid infiltration rate of 0.4 μL/min and lateral liquid access even when spliced with SMFs. Moreover, the fabricated SC-PCF has low transmission loss, low insertion loss, and ignorable bending loss, which are beneficial for constructing an ultra-sensitive and compact all-in-fiber sensing scheme. Furthermore, an absorption sensor and a Sagnac interferometer are demonstrated with their versatile sensing capabilities with MB absorptive molecule, non-specific liquid RI detection, and cTnT molecules. The constructed absorption sensor shows a LOD of 500 nM MB solution, while the SC-PCF based Sagnac interferometer shows a high RI sensitivity of 2849 nm/RIU with great stability and is able to detect 1 ng/mL human cTnT protein. Moreover, *in situ* monitoring of biological binding event on the fiber core is achieved. The demonstrated SC-PCF offers a highly-efficient solution to the construction of flexible and versatile all-in-fiber optofluidic sensing systems with promising applications in chemical and biological analysis for monitoring environment or biological/medical diagnosis.

Conflicts of interest

There are no conflicts to declare.

Acknowledgements

References

1   C. Monat, P. Domachuk and B. J. Eggleton, *Nat. Photonics*, 2007, **1**, 106–114.
2   Y. Yang, A. Q. Liu, L. Lei, L. K. Chin, C. D. Ohl, Q. J. Wang and H. S. Yoon, *Lab Chip*, 2011, **11**, 3182–3187.
3   Y. Shi, L. Liang, X. Q. Zhu, X. M. Zhang and Y. Yang, *Lab Chip*, 2015, **15**, 4398–4403.
4   N. Zhang, H. Liu, A. M. Stolyarov, T. Zhang, K. Li, P. P. Shum, Y. Fink, X. W. Sun and L. Wei, *ACS Photonics*, 2016, **3**, 2275–2279.
5   X. Fan and I. M. White, *Nat. Photonics*, 2011, **5**, 591–597.
6   H. A. Katus, S. Looser, K. Hallermayer, A. Remppis, T. Scheffold, A. Borgya, U. Essig and U. Geuss, *Clin. Chem.*, 1992, **38**, 386–393.
7   H. L. Liu, X. Q. Zhu, L. Liang, X. M. Zhang and Y. Yang, *Optica*, 2017, **4**, 839–846.
8   L. Wei, L. Eskildsen, J. Weirich, L. Scolari, T. T. Alkeskjold and A. Bjarklev, *Appl. Opt.*, 2009, **48**, 497–503.
9   C. Wu, M.-L. V. Tse, Z. Liu, B.-O. Guan, a P. Zhang, C. Lu and H.-Y. Tam, *Analyst*, 2014, **139**, 5422–5429.
10 N. Zhang, G. Humbert, Z. Wu, K. Li, P. P. Shum, N. M. Y. Zhang, Y. Cui, J.-L. Auguste, X. Q. Dinh and L. Wei, *Opt. Express*, 2016, **24**, 419–424.
11 H. W. Lee, M. a Schmidt, P. Uebel, H. Tyagi, N. Y. Joly, M. Scharrer and P. S. J. Russell, *Opt. Express*, 2011, **19**, 8200–8207.
12 C. Wu, M.-L. V. Tse, Z. Liu, B.-O. Guan, C. Lu and H.-Y. Tam, *Opt. Lett.*, 2013, **38**, 3283–3286.
13 N. Zhang, G. Humbert, T. Gong, P. P. Shum, K. Li, J.-L. Auguste, Z. Wu, D. J. J. Hu, F. Luan, Q. X. Dinh, M. Olivo and L. Wei, *Sensors Actuators B Chem.*, 2016, **223**, 195–201.
14 S. Gao, L.-P. Sun, J. Li, L. Jin, Y. Ran, Y. Huang and B.-O. Guan, *Opt. Express*, 2017, **25**, 13305–13312.
15 S. Unterkofler, R. J. McQuitty, T. G. Euser, N. J. Farrer, P. J. Sadler and P. S. J. Russell, *Opt. Lett.*, 2012, **37**, 1952–1954.
16 T. G. Euser, J. S. Y. Chen, M. Scharrer, P. S. J. Russell, N. J. Farrer and P. J. Sadler, *J. Appl. Phys.*, 2008, **103**, 103108.
17 B. M. Zhang, Y. Lai, W. Yuan, Y. P. Seah, P. P. Shum, X. Yu and H. Wei, *Opt. Express*, 2014, **22**, 2675–2680.
18 X. Yang, T. Yuan, P. Teng, D. Kong, C. Liu, E. Li, E. Zhao, C. Tong and L. Yuan, *Lab Chip*, 2014, **14**, 2090–2095.
19 I. H. Malitson, *J. Opt. Soc. Am.*, 1965, **55**, 1205–1209.
20 Z. Xu, K. Duan, Z. Liu, Y. Wang and W. Zhao, *Opt. Commun.*, 2009, **282**, 4527–4531.
21 P. S. J. Russell, *J. Light. Technol.*, 2006, **24**, 4729–4749.
22 P. Russell, *Science (80-.).*, 2003, **299**, 358–362.
23 Z. He, F. Tian, Y. Zhu, N. Lavlinskaia and H. Du, *Biosens. Bioelectron.*, 2011, **26**, 4774–4778.
24 S. Korposh, S. James, R. Tatam and S. Lee, in *Current Developments in Optical Fiber Technology*, eds. S. W. Harun and H. Arof, InTech, Rijeka, 1st edn., 2013,9, p. 238.
25 A. Prabhakar and S. Mukherji, *Lab Chip*, 2010, **10**, 748–754.
26 J. M. Zhu, Y. Shi, X. Q. Zhu, Y. Yang, F. H. Jiang, C. J. Sun, W. H. Zhao and X. T. Han, *Lab Chip*, 2017, **17**, 4025–4030.
27 A. Erdem, K. Kerman, B. Meric and M. Ozsoz, *Electroanalysis*, 2001, **13**, 219–223.
28 B. J.-C. Deboux, E. Lewis, P. J. Scully and R. Edwards, *J. Light. Technol.*, 1995, **13**, 1407–1414.

29 B. Wyrwas and A. Zgoła-Grześkowiak, *J. Surfactants Deterg.*, 2014, **17**, 191–198.

30 S. George and A. Kishen, *J. Biomed. Opt.*, 2007, **12**, 34029.

31 Z. Klika, P. Čapková, P. Horáková, M. Valášková, P. Malý, R. Macháň and M. Pospíšil, *J. Colloid Interface Sci.*, 2007, **311**, 14–23.

32 A. S. Streng, D. De Boer, W. P. T. M. Van Doorn, F. G. Bouwman, E. C. M. Mariman, O. Bekers, M. P. Van Dieijen-Visser and W. K. W. H. Wodzig, *Clin. Chem.*, 2017, **63**, 563–572.

33 M. Kitamura, N. Hata, T. Takayama, A. Hirayama, M. Ogawa, A. Yamashina, H. Mera, H. Yoshino, F. Nakamura and Y. Seino, *J. Cardiol.*, 2013, **62**, 336–342.